Dynamic optical rectification and delivery of active particles

Soft Matter

ARTICLE TYPE

Cite this: DOI: 00.0000/xxxxxxxxxx

Dynamic optical rectification and delivery of active particles†

Nick Koumakis,[a] Aidan T. Brown,[a] Jochen Arlt,[a] Samuel E. Griffiths,[a] Vincent A. Martinez,[a] and Wilson C. K. Poon[a]

Received Date
Accepted Date

DOI: 00.0000/xxxxxxxxxx

We use moving light patterns to control the motion of *Escherichia coli* bacteria whose motility is photo-activated. Varying the pattern speed controls the magnitude and direction of the bacterial flux, and therefore the accumulation of cells in up- and down-stream reservoirs. We validate our results with two-dimensional simulations and a 1-dimensional analytic model, and use these to explore parameter space. We find that cell accumulation is controlled by a competition between directed flux and undirected, stochastic transport. Our results point to a number of design principles for using moving light patterns and light-activated micro-swimmers in a range of practical applications.

1 Introduction

Active colloids[1] are fundamentally interesting, exhibiting phenomena not found in equilibrium systems such as currents and unique kinds of pattern formation[2]. Such phenomena have been applied, e.g., to concentrate particles[3] or separate them by size, actuate micro-machines[4], or self-assemble microstructures. For example, V-shaped 'funnel gates' fabricated using soft lithography can rectify the motion of randomly-swimming bacteria[3], producing steady currents or spatial patterns. Similar effects can be achieved by applying a spatial light pattern to bacteria or other active colloids whose speed v depends on the intensity of incident light, I. If $\mathrm{d}v/\mathrm{d}I > 0$, bacteria in illuminated regions swim until they encounter a darker region, where they are slowed down. Cells then accumulate in the dark regions because they swim out of the light regions and stop in the dark. Quantitatively, this leads to the relationship $\rho v = \text{constant}$[5,6] where ρ is the spatially varying bacterial concentration.

This technique for 'painting patterns with bacteria' has been demonstrated using *Escherichia coli* in which the proton motive force (PMF) driving swimming is generated by light-powered proteorhodopsin (PR)[6–8]. Potential applications include directing swimmers into compartments[3,9] to actuate micro-mechanical components[4]. Such 'bacterial painting' becomes significantly more versatile if the template is dynamic. Thus, globally time-varying light fields projected onto PR-driven *E. coli* can 'erase' and 're-paint' patterns[7]. Here, we study the response of PR-driven *E. coli* to spatio-temporally varying light fields, specifically, wave-like propagating periodic patterns of illumination. By using a combination of experiments, theory and simulations we uncover a rich array of often counter-intuitive phenomena.

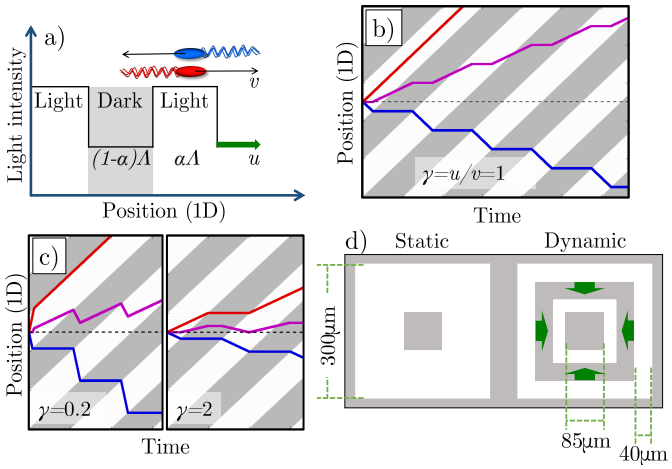

Fig. 1 (a) 1D schematic of a translating square-wave light field with co- (red) and counter-moving (blue) bacteria. (b) Kymograph of a light field moving at speed u (duty cycle $\alpha = 0.5$) with light regions as white and dark ones with grey stripes and with trajectories of non-tumbling right (red) and left (blue) swimmers at speed $v = u$ (i.e. $\gamma \equiv u/v = 1$) and the mean trajectory (magenta). (c) Kymograph for $\gamma = 0.2$ and 2, and $\alpha = 0.5$. (d) Schematic of the 2D light pattern in our experiments.

To motivate our work, consider a 1D model solvable by inspection. Bacteria swim right ($+x$, $\rightharpoonup$) or left ($-x$, $\leftharpoondown$) at speed v when illuminated, and stop completely in the dark; the (equal) $\rightharpoonup$ and $\leftharpoondown$ populations do not exchange. Now impose and translate at speed $u > 0$ a square-wave light pattern, Fig. 1a. If $\gamma = u/v = 1$,

[a] SUPA and School of Physics & Astronomy, The University of Edinburgh, James Clerk Maxwell Building, Peter Guthrie Tait Road, Edinburgh EH9 3FD, Scotland, UK

† Electronic Supplementary Information (ESI) available: [details of any supplementary information available should be included here]. See DOI: 00.0000/00000000.

$\rightharpoonup$ cells keep up with the moving light field in steady state, and so maintain their speed v, whereas $\leftharpoondown$ cells spend only some of their time in the light, determined by the duty cycle (fractional on time) of the pattern, α. This results in a net positive cell flux, i.e., a light pattern translating at $\gamma = 1$ rectifies the cells' motion and transports them with the pattern. We can represent this behaviour in a space-time plot (kymograph), Fig. 1b.

Optimal rectification is obtained for $\gamma \approx 1$: For $\gamma \ll 1$, $\rightharpoonup$ cells remain trapped at the slowly-moving light-dark interface, while the $\leftharpoondown$ cells move faster through the light regions; For $\gamma \gg 1$, the light field moves much faster than the cells, so both $\rightharpoonup$ and $\leftharpoondown$ cells spend $\approx 50\%$ time in the dark and the light. Either way, the net flux falls, Fig. 1c. This qualitative picture has been quantified previously in simulations and theoretically[10,11]. Counter-intuitively, these works also predicted that a *reversal* of the flux direction is possible for $\gamma \ll 1$, and showed that this was dependent on other parameters such as the bacterial tumbling rate[10] or the speed of bacteria in the dark[11].

In this paper, we first perform bacterial experiments designed to quantitatively test these theoretical predictions. Our experiments reproduce the optimal rectification suggested by the intuitive picture, and identify flux reversal at low pattern speeds. Simulations of our system quantitatively reproduce our experimental results, but only when we include a biological delay in the bacterial response to light, and translational thermal diffusion of the bacteria. We go on to explore the wider parameter space using a one-dimensional analytical theory. This allows us to explain various mechanisms for flux reversal, controlled, e.g., by rotational diffusion or the duty cycle of the pattern. Further, we show that the parameter dependence of the steady-state downstream accumulation of bacteria, i.e., their ability to form patterns, can be quite different, and even reversed, from the parameter dependence of the flux in periodic boundary conditions, which theoretical studies generally discuss[10,11]. Based on these findings, we articulate design principles for the transport of light-activated swimmers using moving patterns of illumination.

2 Materials and methods

The bodies of *E. coli* bacteria[12] are $\approx 2\mu\text{m} \times 1\mu\text{m} \times 1\mu\text{m}$ spherocylinders. They swim by using their PMF (of $\approx -150\,\text{mV}$) to power membrane-embedded rotary motors which rotate $\approx$ 7-10μm helical flagella. Unusually for bacteria, *E. coli* can generate a PMF without external nutrients[13] by using internal resources and O_2 to pump protons out of the cell. Without O_2, swimming ceases[12] unless there is another source of PMF, as in cells expressing PR[14], a photon-driven proton pump. Thus, under anaerobic conditions, PR-expressing *E. coli* cells swim only when illuminated, which is analogous to synthetic light-activated swimmers[15,16].

We inserted a PR-bearing plasmid into *E. coli* AB1157, and deleted the *che*Y gene and the *unc* operon encoding the ATP synthase complex to give strain AD10[7]. The former deletion turns wild-type run-and-tumblers into smooth swimmers, while the latter gives fast stopping whenever illumination ceases[7].

Overnight cultures were grown aerobically in 10 ml Luria–Bertani broth at 30^{o}C. A fresh culture was inoculated at 1:100 dilution of the pre-grown cells in 35 ml tryptone broth and grown for 4 h. The production of PR was induced by adding arabinose to a concentration of 1 mM, as well as the necessary cofactor all-trans-retinal to 10μM in the growth medium. Cells were incubated under the same conditions for a further hour to allow protein expression to take place and then transferred to motility buffer. A single filtration was used to prepare high density stock solutions (optical density$\approx$10) which were diluted with phosphate motility buffer (MB, pH 7.0, 6.2 mM K_2HPO_4, 3.8 mM KH_2PO_4, 67 mM NaCl and 0.1 mM EDTA) to an optical density ≈ 6 at 600 nm (≈ 0.8 vol.% cell bodies[12]). 2μL aliquots sealed into 20μm-thick, $\approx$ 10 mm wide, flat glass capillaries were observed in phase contrast under red illumination using a PF 10$\times$/0.3 NA objective on a Nikon TE2000 microscope. Movies were recorded with a high speed CMOS MC1462 Mikrotron camera. Swimming stopped a few minutes after sealing due to O_2 depletion.

After leaving these cells in the dark for a further 10 min, uniform green illumination was turned on (510-560 nm, corresponding to peak PR absorption; $\approx 5\ \text{mW}\,\text{cm}^{-2}$ at the sample). Differential dynamic microscopy (DDM)[17,18] returned an increasing mean swimming speed $\bar{v}$, saturating at $\approx 6.5\mu\text{m}\,\text{s}^{-1}$, with standard deviation $\approx 2.5\mu\text{m}\,\text{s}^{-1}$ and a typical fraction $\beta \approx 25\%$ of non-motile bacteria ($\bar{v}$ is averaged over the motile bacteria only). The non-motile bacteria have diffusivity $D_\text{T} \approx 0.15\mu\text{m}^2\,\text{s}^{-1}$. In this work, we use the terms 'motile/non-motile' to refer to cells that are able/unable to swim in the presence of green light, while the descriptors 'swimmers/non-swimmers' are reserved for those motile cells that are transiently powered/not-powered by external illumination.

A spatial light modulator projected a 4×4 array of static and dynamic patterns onto this initially uniform field of swimmers and non-motile cells. Each pattern featured a central dark square (side $l = 85\mu$m) inside an outer square (side $L = 300\mu$m), Fig. 1d. In the static pattern, the square annulus was uniformly illuminated. The dynamic pattern comprised concentric square annuli of equal width $\Lambda/2 = 40\mu$m ($\alpha = 0.5$) propagating inwards at speed u. The area outside the patterns was dark in all cases. We chose a square-wave intensity pattern because its predicted flux is higher than other waveforms previously considered, e.g., sinusoidal[11]. Moreover, the fact that the swimming speed is nonlinearly dependent on the light intensity[7] means that any pattern apart from a square-wave pattern will be distorted, complicating the experiment and analysis.

In our setup, the local intensity variance in the microscopy image, σ^2, has previously been found to be proportional to the local cell density[7] (See SI for details). Here, we are interested in the density $\rho_\text{in}(t)$ of motile cells in the central square of the pattern

$$\rho_\text{in}(t) = f\sigma^2_\text{in}(t)\left[1 - \beta_\text{in}(t)\right], \tag{1}$$

where f is a constant of proportionality, and σ^2_in and β_in are the local variance in pixel intensity averaged over the inner square, and the motile fraction in the inner square, respectively. We assume zero net transport of non-motile cells, i.e., $\beta_\text{in}(t)\sigma^2_\text{in}(t) = \beta_\text{in}(0)\sigma^2_\text{in}(0)$, and calculate the relative accumulation of motile

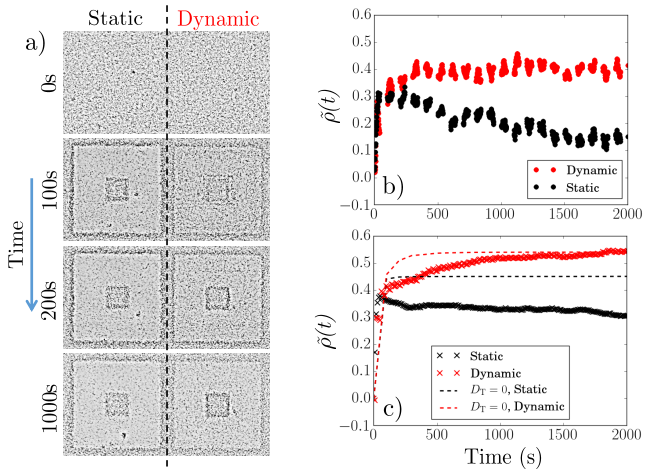

Fig. 2 (a) Phase contrast microscopy snapshots of a static pattern, and a dynamic pattern with $u = 2.25$ μm/s ($\gamma = u/\bar{v} = 0.35$, with $\bar{v} = 6.5$ μm/s). (b) Experimental normalized density $\tilde{\rho}$ at the center of the pattern as a function of time for static and dynamic patterns. (c) 2D simulated $\tilde{\rho}$ for a dynamic ($u = 2.0$ μm/s, $\gamma = 0.31$) and a static pattern, with (dots) and without (dashes) thermal motion.

cells averaged over the inner square:

$$\tilde{\rho}(t) \equiv \frac{\rho_{\rm in}(t) - \rho_{\rm in}(0)}{\rho_{\rm in}(t) + \rho_{\rm in}(0)} = \frac{\sigma^2_{\rm in}(t) - \sigma^2_{\rm in}(0)}{\sigma^2_{\rm in}(t) + \sigma^2_{\rm in}(0)(1 - 2\beta_{\rm in}(0))}. \quad (2)$$

Initially, $\rho_{\rm in}(0) = \rho_{\rm out}(0) = \rho_0$, the uniform motile density everywhere. Subsequently, we find that the outer motile cell density stays approximately constant, i.e., $\rho_{\rm out}(t) \sim \rho_0$ (see SI), so that $\tilde{\rho}(t)$ also corresponds to the contrast between the inside and outside of the pattern, i.e., $\tilde{\rho}(t) = (\rho_{\rm in}(t) - \rho_{\rm out}(t))/(\rho_{\rm in}(t) + \rho_{\rm out}(t))$. Our choice of normalization means that $\tilde{\rho} = \pm 1$ for complete rectification in the inwards or outwards directions respectively.

3 Results

3.1 Rectification in 2D experiments and simulations

Fig. 2 shows data for $u = 2.25 \mu{\rm m\,s}^{-1}$, corresponding to $\gamma = 0.35$. Imposing a static pattern 'paints' a central dark square and the outer square acquires a dark edge, Fig. 2a, as previously[7], because cells in the bright (B) annulus swim into the dark (D) central square and outer regions in roughly equal numbers and stop upon arrival. Because the central square is much smaller than the outer region this initial influx of swimmers from the bright annulus gives a sharp increase in $\rho_{\rm in}$ and therefore $\tilde{\rho}$, Fig. 2b (•). Thereafter, $\tilde{\rho}$ decreases slowly as accumulated non-swimmers diffuse back out into the bright annulus and swim to the outside of the annulus. Presumably, at long times, a steady state obtains where the B → D active flux balances the D → B diffusive flux, so that we expect $\rho_{\rm in}(t \to \infty) \approx \rho_{\rm out}(t \to \infty) = \rho_0$, and $\tilde{\rho}(t \to \infty) = 0$. However, we cannot reach this limit experimentally because bacteria slow down and begin to aggregate with time, possibly due to accumulated photo-damage. The contrast in the steady-state 'static painting' is due to the annulus, inhabited by a small amount of non-motile cells and few swimmers in transit, so that $\rho_{\rm ann} \ll \rho_0$.

The dynamic light pattern also accumulates cells in the central square, Fig. 2a. The difference from the static case, already visible in the snapshots but highlighted in Fig. 2b, is that $\tilde{\rho}(t)$ does *not* decay after the initial increase, but reaches instead a finite steady-state value. This enhancement of accumulation depends non-monotonically on $\gamma = u/v$, Fig. 3a, and, counter-intuitively, it reverses sign at $\gamma \ll 1$: cells are swept *out* of the central region ($\tilde{\rho} < 0$). Both of these features are clearly illustrated in Fig. 3c, which shows that at both t =500 s and t =4000 s, $\tilde{\rho}$ is peaked as a function of γ, and that at the later time $\tilde{\rho} < 0$ when $\gamma \lesssim 0.05$ (see SI movie 1).

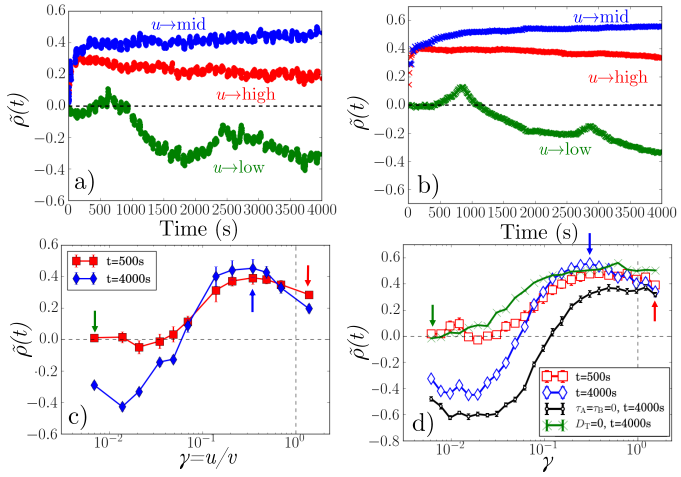

Fig. 3 (a) Experimental time-dependent normalized density $\tilde{\rho}(t)$ for pattern speeds u =0.045, 2.25, 9 μm/s ($\gamma = 0.007,\ 0.35,\ 1.4$). (b) 2D simulations ($\gamma = 0.006,\ 0.31,\ 1.54$). (c) Experimental $\tilde{\rho}$ as a function of pattern speed for indicated times from experiments. (d) As in (c) but from simulations, and also results for $D_T = 0$ and τ_A=τ_B=0. Arrows in (c) and (d) correspond to the γ from (a) and (b). Error bars in c) and d) refer to the standard deviation of the values taken in a ±100s window.

To explore these features, we simulated 2×10^4 non-interacting swimmers in a 600×600 μm^2 periodic box. Particle speeds v_i are drawn from an experimental Schultz distribution for our bacteria[17,18] (mean = $6.5 \mu{\rm m\,s}^{-1}$, 40% standard deviation). The dynamics of particle i obeys

$$\dot{\mathbf{r}}_i = v_i A_i B_i \mathbf{p}_i + \sqrt{2D_T}\xi_T, \quad (3)$$

$$\dot{\theta}_i = \sqrt{2D_R}\xi_R, \quad (4)$$

$$\dot{A}_i = (I(\mathbf{r}_i) - A_i)/\tau_A, \quad (5)$$

$$\dot{B}_i = (I(\mathbf{r}_i) - B_i)/\tau_B, \quad (6)$$

with $\mathbf{r}_i$ and $\mathbf{p}_i = (\cos\theta_i, \sin\theta_i)$ its position and propulsion direction respectively. ξ_T is a two- and ξ_R is a one-dimensional unit-variance temporally-uncorellated Gaussian noise term (in each direction for ξ_T). Translational, $D_T = 0.15 \mu{\rm m}^2\,{\rm s}^{-1}$, and rotational, $D_R = 0.05\,{\rm s}^{-1}$, diffusivities reflect experimental values (see SI). The normalized light intensity, $I(\mathbf{r}_i, t) = 1$ for bright and 0 for dark. The two dynamical variables A and B reflect the observation[7] that two independent, internal processes control the response of our cells to changes in the intensity of external illumination. We independently measured $\tau_A = 1.6$ s and $\tau_B = 100$ s (see SI). Note that in the instant-response limit ($\tau_A = \tau_B = 0$) this model reduces to

the popular 2-dimensional active-Brownian-particle (ABP) model that was previously used to study the effect of translating light patterns[10,11].

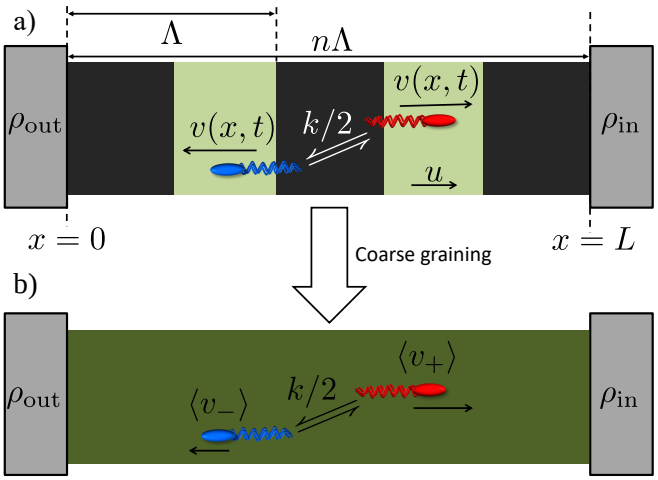

Fig. 4 Schematic of coarse graining for 1-dimensional model. a) Bacteria swim at speed $v(x,t)$ and tumble at rate k in a light pattern translating at speed u between two reservoirs with steady-state bacterial concentration ρ_{out} and ρ_{in}. b) After coarse graining, the bacteria are considered to swim uniformly at the average speeds $\langle v_+\rangle$ and $\langle v_-\rangle$ they would obtain from the same pattern moving with periodic boundary conditions.

Our simulations reproduce the observed rise and decay in $\tilde{\rho}(t)$ for the static pattern, Fig. 2c (×). The saturation behavior for the dynamic pattern is also reproduced, Fig. 2c (×). Most visibly in the decay of the static case, the simulated dynamics is slower than experiments, by a factor of ≈ 2, possibly due to our neglect of cell-cell interactions, which are expected to lead to an increased apparent diffusivity[19]. Even so, the semi-quantitative agreement is gratifying given the simplicity of our model.

We also claimed that the diffusion of cells that had stopped swimming in the dark was responsible for the observed non-monotonicity in $\tilde{\rho}(t)$ of the static pattern, Fig. 2b (•). Simulations confirm this: setting $D_{\text{T}} = 0$ removes the drop in $\tilde{\rho}(t)$, Fig. 2c (- - -). The effect of removing diffusion on the dynamic pattern is to render the rise to saturation significantly more rapid, Fig. 2c (- - -). Thus, a dynamic pattern has to work against translational thermal diffusion, as identified previously[10] (see SI movies 2, 3 and 4).

The simulations account well for the dynamics of $\tilde{\rho}(t)$ at our selected experimental u values, Fig. 3b, including the oscillations at low u with a characteristic time $= \Lambda/u \sim 2\times10^3$ s. These oscillations occur because as the band of light approaches the dark centre, swimmers in the band are able to 'tunnel through' and stop in the centre, increasing the accumulation transiently, until the leading edge of the light band reaches the outer edge of the dark centre. Now, thermal diffusion can transport cells from the darkness to the light, whereupon they swim outwards, reducing ρ in the central dark area (see SI movies 5 and 6).

Similarly, $\tilde{\rho}(\gamma)$ is well reproduced over two orders of magnitude in γ, for both $t = 500$ s and 4000 s, see Fig. 3c-d. In both cases $\gamma \approx 0.3$ is optimal for accumulation, and flux reversal (drainage of the central square) occurs if $\gamma \lesssim 0.1$. Importantly, with $D_{\text{T}} = 0$, Fig. 3d (green), simulations show no flux reversal: bacteria transported inwards cannot escape the inner square (see SI movie 7). Nor does taking the instant-response limit $\tau_{\text{A,B}} = 0$ give quantitative agreement, Fig. 3d (black).

3.2 Exploring parameter space with a 1D analytic model

So far we have studied the effect of varying one parameter, the pattern speed $u = \gamma v$ using 2D experiments and simulations. We now turn away from experiments to construct an idealized 1D analytic model, which will allow us to explore the wider parameter space. Our calculations are based on recent analytical results for light-activated particles in a 1D periodic moving light field[11], which is the one-dimensional version of our 2-dimensional simulation model, but with instant bacterial response, no translational diffusion, and rotational diffusion replaced by tumbling (the only possibility in 1D). The 1-dimensional model was originally solved for a square wave in periodic boundary conditions, and used to show that flux inversion can occur if the bacteria have a finite swimming speed in the dark. Here, our bacteria do not swim in the dark, so we look at other mechanisms for flux inversion, notably caused by the pattern's duty cycle, α, or by the tumbling rate of the bacteria. We also extend the analysis to account for the non-periodic boundaries in our 2D experiments, which permit accumulation.

In the original theory[11], active point particles move right or left at speed v in the light and v' in the dark, but we set $v' = 0$ here. Particles reorient independently at rate k, which can be viewed as a tumbling or rotational diffusion rate, non-dimensionalised as $\kappa \equiv k\Lambda/u$ (tumbling and rotational diffusion are indistinguishable in 1D). A periodic, square light pattern is imposed, moving at speed $u > 0$, in whose comoving frame are periodic boundary conditions (BCs) at $x = 0$ and $x = \Lambda$, with $[0, \alpha\Lambda)$ light and $[\alpha\Lambda, \Lambda)$ dark. The Fokker-Planck equation (FPE) for this system with $\alpha = 0.5$ was solved[11] to yield the average transport velocity, $\langle v\rangle$ (equivalently, the flux), in periodic boundary conditons.

In our experiments, we do not have periodic boundary conditions, and we do not measure flux: instead we probe the density difference between different regions, which is also the relevant variable for pattern formation. We therefore extend the results of[11] (see SI) into a coarse-grained theory to predict density differences. In detail, we calculate the concentration difference between either end of a finite square-wave illumination pattern of n (not necessarily integer) periods moving from an 'outer' reservoir at $x = 0$ to an 'inner' reservoir at $x = L = \Lambda n$, see Fig. 4a. In the moving region, $0 < x < L$, we coarse-grain over the periodic dynamics by approximating all the bacteria in this region as having uniform speeds given by the mean speeds $\langle v_+\rangle$ and $\langle v_-\rangle$ that ⇀ and ↽ bacteria, respectively, would have in the equivalent periodic pattern, see Fig. 4. This approximation should be valid as long as there are a sufficient number n of periods in the moving pattern. The mean speeds $\langle v_+\rangle$ and $\langle v_-\rangle$ are obtained in the same way as the overall mean speed $\langle v\rangle = (\langle v_+\rangle - \langle v_-\rangle)/2$ was in ref. [11]. We give expressions for and outline the calculation of these quantitities in the SI.

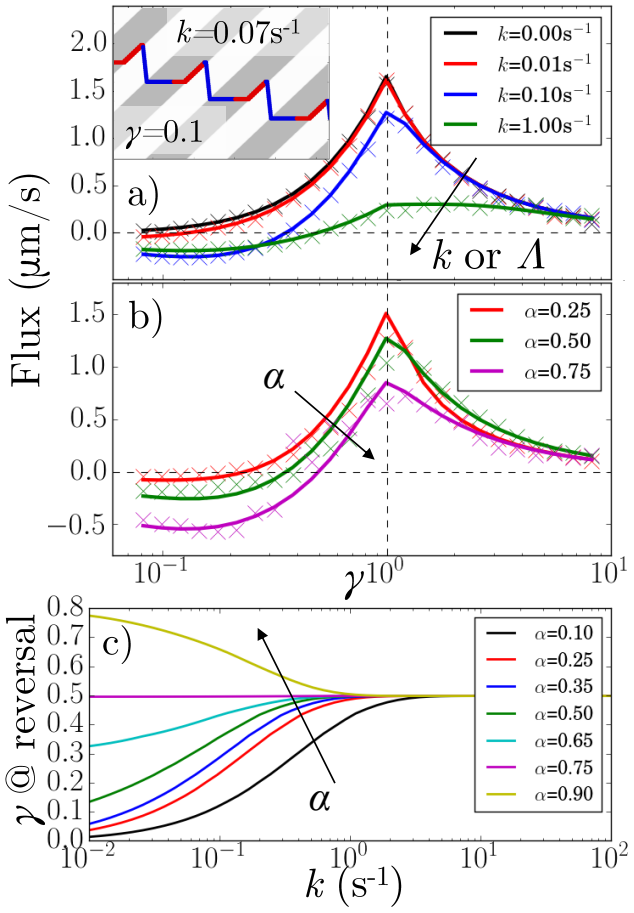

Fig. 5 (a) 1D theory (lines) and simulations (points) of average particle velocity (or flux) *vs* pattern speed for $\alpha = 0.5$ and $k = 0, 0.01, 0.1$ and $1\,\mathrm{s}^{-1}$. Inset: kymograph of a particle tumbling periodically at $k = 0.07\,\mathrm{s}^{-1}$ with $\alpha = 0.5$ and $\gamma = 0.1$. (b) As in (a) but for $k = 0.01\,\mathrm{s}^{-1}$ and $\alpha = 0.25, 0.5$ and 0.75. (c) Predicted critical γ for flux reversal, γ^*, *vs* k for different α (in legend).

We are interested in concentration differences in steady state, so we write down the resulting FPE for the time-invariant (coarse grained) probability densities $\phi_\pm$ in the lab frame

$$0 = \frac{\partial \phi_+}{\partial t} = -\langle v_+ \rangle \frac{\partial \phi_+}{\partial x} + \frac{k}{2}(\phi_- - \phi_+)\,,$$
$$0 = \frac{\partial \phi_-}{\partial t} = \langle v_- \rangle \frac{\partial \phi_-}{\partial x} + \frac{k}{2}(\phi_+ - \phi_-)\,. \qquad (7)$$

where the first term on the right-hand side accounts for advection due to swimming, and the second accounts for tumbling between the two orientations. BCs account for the reservoirs: the flux $j_+(0)$ of $\rightharpoonup$ particles into the light-pattern at $x = 0$ is

$$j_+(0) = \phi_+ \langle v_+ \rangle = C\rho_{\mathrm{out}}\,, \qquad (8)$$

with ρ_{out} the bacterial density in the $x = 0$ reservoir, and C a constant accounting for the rate at which bacteria exit the reservoirs (the value of C does not affect the steady state provided $C > 0$; this will be the case as long as there is any translational diffusion, though we do not need to include this explicitly in the model). Similarly, the flux of $\leftharpoondown$ particles out of the $x = L$ reservoir is

$$j_-(L) = -\phi_- \langle v_- \rangle = -C\rho_{\mathrm{in}}\,. \qquad (9)$$

The other condition is that steady state requires zero net flux everywhere, so $j = j_+ + j_- = \langle v_+ \rangle \phi_+ - \langle v_- \rangle \phi_- = 0$.

Solving Eq. (7) subject to these conditions yields an exponential density distribution across the moving part of the light-field

$$\phi_+ = \frac{C\rho_{\mathrm{out}}}{\langle v_+ \rangle} \exp\left[\frac{kx\langle v \rangle}{\langle v_+ \rangle \langle v_- \rangle}\right],$$
$$\phi_- = \frac{C\rho_{\mathrm{out}}}{\langle v_- \rangle} \exp\left[\frac{kx\langle v \rangle}{\langle v_+ \rangle \langle v_- \rangle}\right], \qquad (10)$$

and an expression for the parameter of interest, the steady-state accumulation $\tilde{\rho}_\infty = \tilde{\rho}(t \to \infty)$ (see Eq. (2))

$$\tilde{\rho}_\infty = \tanh\left(\frac{kn\Lambda\langle v \rangle}{2\langle v_+ \rangle \langle v_- \rangle}\right). \qquad (11)$$

This result can be understood as a balance between the persistent particle flux, $\langle v \rangle$, and stochastic events where individual particles traverse the pattern against the flux. This can be seen most clearly in the case where the flux is strong in one direction, with bacteria only occasionally moving against the flow, e.g., if $\langle v_- \rangle \ll \langle v_+ \rangle$. In this case, the probability of a bacterium which leaves the outer reservoir reaching the inner reservoir is $p_+ \sim 1$, whereas the probability p_- of a bacterium passing in the opposite direction without returning to the inner reservoir is much smaller, and is approximately equal to the probability that zero left-to-right tumbles occur within the time $\tau_- = n\Lambda/\langle v_- \rangle$ taken for the bacterium to traverse this distance, i.e., $p_- \sim \exp(-k\tau_-/2)$. The steady state requirement then gives $\rho_{\mathrm{in}}/\rho_{\mathrm{out}} = p_+/p_- \sim \exp[kn\Lambda/(2\langle v_- \rangle)]$, yielding $\tilde{\rho}_\infty \sim \tanh[kn\Lambda/(4\langle v_- \rangle)]$, which is in fact the limiting form of Eq. (11) for $\langle v_- \rangle \ll \langle v_+ \rangle$.

These theoretical results predict what happens when we vary α and κ (by changing k or Λ or both), Fig. 5. In particular, the flux reverses at a critical $\gamma^* < 1$, Fig. 5a,b, that is k and α-dependent, Fig. 5c. Under our $v' = 0$ conditions, such reversal requires a finite k (whereas for $v' > 0$, reversal can occur at $k = 0$[11]).

The speed reversal at $k > 0$ occurs, Fig. 5a, because of an asymmetry in the effect of tumbling on the $\rightharpoonup$ and $\leftharpoondown$ parts of the trajectory, which is illustrated in the inset for regular (period $1/k$) tumbling. Tumbling effectively retards particles more during $\rightharpoonup$ (red) periods because they then become un-trapped from the moving interface and so spend significant amounts of time static in the dark. The effect on the $\leftharpoondown$ (blue) part of the trajectory is weaker because this part of the trajectory is already significantly in the dark even without tumbles, so tumbling will not disturb the relatively rapid runs through the light, lasting $\tau_{\mathrm{light}} = \Lambda\alpha/(u+v)$ until the tumbling rate increases above the rate of this process, i.e., when $k\tau_{\mathrm{light}} \gtrsim 1$.

How the duty cycle α affects reversal, Fig. 5b, is illustrated by the kymographs in Fig. 6a. For increasing α, $\leftharpoondown$ particles spend longer in the light (so the blue curve becomes steeper), whereas $\rightharpoonup$ particles trapped at the boundary are unaffected (the red curve stays the same); hence the reversal point γ^* shifts to higher values

with increasing α.

Perhaps counter-intuitively, the accumulation $\tilde{\rho}_\infty$, Fig. 6b, c, is not trivially related to the behavior of the flux, Fig. 5a, b. The case of $\alpha = 0.5$ is striking: the accumulation generally increases with increasing k even though the flux decreases. This is mainly because as the tumbling rate increases, the probability of a bacterium moving from one reservoir to the other, without tumbling, decreases; hence, the number of events where bacteria 'hop' back over the moving light field against the net flow also decreases. As the tumbling rate rises, it thus becomes easier to maintain a concentration gradient, and this effect turns out to be stronger than the simultaneous decrease of the flux.

To validate our analytics, we simulated a 1D system obeying the same dynamical equations already used for 2D, but with the reorientation, Eq. 4, replaced by a Poissonian tumbling process, and with instant bacterial response, $\tau_A = \tau_B = 0$. This reproduced the predicted fluxes exactly, Figs. 5a,b, as before[11]. To extract $\tilde{\rho}$, we used simulations of a finite system, adding a small $D_\mathrm{T} = 0.01\,\mu\mathrm{m}^2\,\mathrm{s}^{-1}$ to allow the particles to escape 20μm-long reservoirs. These simulations only approximately reproduced the theory, Figs. 6b,c. This is reasonable, as the theory itself is an approximation and we expect it to be exact only in the limit of (i) many periods, i.e., $n \gg 1$, where the BCs become less important, and (ii) for limited accumulation each period, i.e., for $k\Lambda\langle v\rangle/(\langle v_+\rangle\langle v_-\rangle) \ll 1$, where it is valid to use a periodic approximation for the cell density distribution.

These results suggest that by tuning α and κ, it should be possible to exercise a great deal of control over how the accumulation and flux vary with γ. This is significant because polydispersity in e.g., speed and rotational diffusion rates are unavoidable, so that one will be dealing with a wide γ distribution in practice, and the ideal pattern design will depend on the goal. For example, concentrating all bacteria in a single target region requires bacteria with a wide range of speeds to be strongly rectified in the same direction, corresponding to the wide γ plateau seen at low α or high Λ in Fig. 6b, c. Alternatively, to separate a sample on the basis of speed when there is also polydispersity in tumbling or rotational diffusion, the value of $\alpha = 0.75$ would be ideal, as the reversal point is then independent of k, see Fig. 5c.

4 Summary and conclusions

Recent numerical[10] and analytical work[11] has explored the effect of moving patterns of light-dark illumination on light-activated swimmers, and predicted the rectification of the random motion of swimmers in the direction of the moving light pattern, and a counter-intuitive regime of reverse rectification at low pattern speeds. We have performed experiments and simulations in 2D to verify that rectification in both directions does indeed occur. The simulations included a finite bacterial response time with two timescales accounting for distinct biological processes, which we found was necessary to faithfully reproduce the experimental results.

We have also generalized the recent 1-dimensional analytic theory[11] to predict not only the swimmer flux, but differences in swimmer densities for different spatial regions, the latter being a more natural experimental variable, and the variable directly relevant to pattern formation. We used this 1D theory to explore a wide parameter range and considered in detail two mechanisms of flux inversion: via bacterial tumbling, and via asymmetry in the waveform (i.e. the duty cycle α). To the best of our knowledge, the effects of waveform asymmetry have not been previously considered in the theoretical or simulation literature[10,11]. We expect that the ability to achieve precise control of bacterial flux by several means will allow for crucial flexibility in future studies.

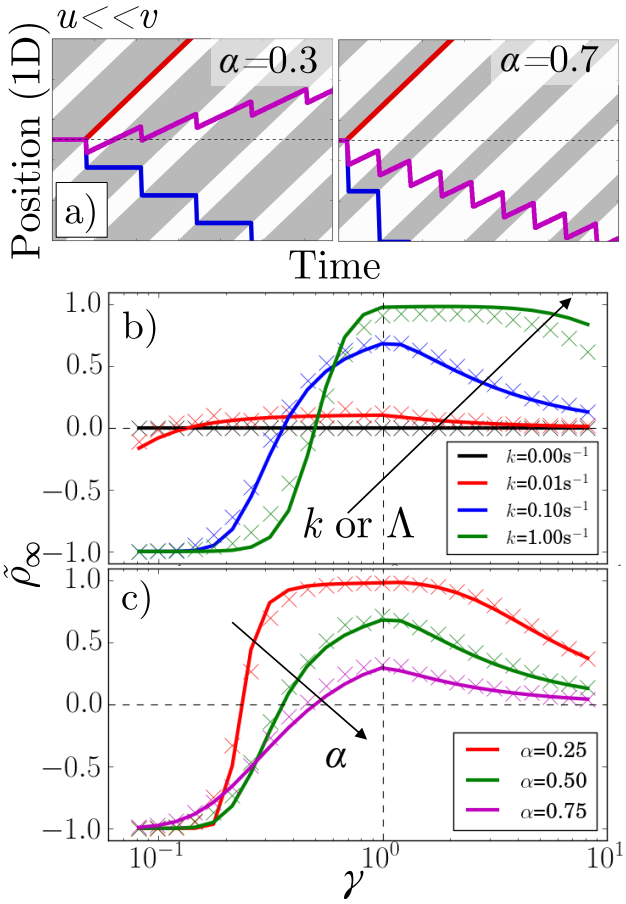

Fig. 6 (a) Kymographs for $\alpha = 0.3$ and $\alpha = 0.7$ with traces of non-tumbling particles moving left (blue) and right (red) for $\gamma \ll 1$. Magenta: the average of the two tracks. (b) 1D simulation and theory of $\tilde{\rho}$ *vs* pattern speed for $\alpha = 0.5$ and $k = 0, 0.01, 0.1$ and $1\,\mathrm{s}^{-1}$. (c) As in (b) but for $k = 0.01\,\mathrm{s}^{-1}$ and $\alpha = 0.25, 0.5$ and 0.75. The colour coding of b) follows that of fig. 5a, while c) follows that of fig. 5b and c.

Indeed, our results point to a number of design principles for particle transport using moving light fields. If the target application requires accumulation, $\gamma \approx 1$ is a necessity, however any light control delays, i.e. deviations from $\tau_A = \tau_B = 0$ are expected to shift the γ of optimum accumulation. Maximal accumulation is also achieved by minimizing the tumble rate and regulating α. Additionally, e.g., if the possibility of flux reversal is important, it will be necessary to use *Brownian* particles, because setting $D_\mathrm{T} = 0$ produced no reversal in our simulations. It is likely that some, if not all, of these principles will be applicable more widely to the control of active particles in other kinds of spatiotemporally-varying fields, e.g., electrical[20] or ultrasound[21]. Spatiotemporally-varying fields, in turn, may become a standard

component in developing applications such as the separation of polydisperse mixtures, the directed-assembly of active particles, and the dynamic actuation and control of microscopic machines.

Acknowledgements

We thank Teun Vissers and Mike Cates for discussions. NK was part-funded by the EU (H2020-MSCA-IF-2014, ActiDoC No. 654688). AB received funding from UK EPSRC (EP/S001255/1). All except SEG received funding from UK EPSRC (EP/J007404/1) and ERC (Advanced Grant ERC-2013-AdG 340877-PHYSAP). SEG held an EPSRC studentship. The data will be available on the University of Edinburgh DataShare open access data repository.

Notes and references

1 W. C. K. Poon, *Physics of Complex Colloids*, IOS Press, Amsterdam, 2013, pp. 317–386.

2 M. E. Cates, *Rep. Prog. Phys.*, 2012, **75**, 042601.

3 P. Galajda, J. Keymer, P. Chaikin and R. Austin, *J. Bact.*, 2007, **189**, 8704–8707.

4 R. Di Leonardo, L. Angelani, D. Dell'Arciprete, G. Ruocco, V. Iebba, S. Schippa, M. Conte, F. Mecarini, F. De Angelis and E. Di Fabrizio, *Proc. Natl. Acad. Sci. (USA)*, 2010, **107**, 9541–9545.

5 J. Tailleur and M. E. Cates, *Phys. Rev. Lett.*, 2008, **100**, 218103.

6 J. Arlt, V. A. Martinez, A. Dawson, T. Pilizota and W. C. K. Poon, *Nature Communications*, 2019, **10**, 2321.

7 J. Arlt, V. A. Martinez, A. Dawson, T. Pilizota and W. C. K. Poon, *Nat Commun.*, 2018, **9**, 768.

8 G. Frangipane, D. Dell'Arciprete, S. Petracchini, C. Maggi, F. Saglimbeni, S. Bianchi, G. Vizsnyiczai, M. L. Bernardini and R. Di Leonardo, *eLife*, 2018, **7**, e36608.

9 N. Koumakis, A. Lepore, C. Maggi and R. Di Leonardo, *Nat. Commun.*, 2013, **4**, 2588.

10 A. Geiseler, P. Hänggi, F. Marchesoni, C. Mulhern and S. Savel'ev, *Phys. Rev. E*, 2016, **94**, 012613.

11 C. Maggi, L. Angelani, G. Frangipane and R. Di Leonardo, *Soft Matter*, 2018, 4958–4962.

12 J. Schwarz-Linek, J. Arlt, A. Jepson, A. Dawson, T. Vissers, D. Miroli, T. Pilizota, V. A. Martinez and W. C. K. Poon, *Colloids Surf. B*, 2016, **137**, 2–16.

13 J. Adler and B. Templeton, *J. Gen. Microbiol.*, 1967, **46**, 175–184.

14 J. M. Walter, D. Greenfield, C. Bustamante and J. Liphardt, *Proc. Natl. Acad. Sci. USA*, 2007, **104**, 2408–12.

15 I. Buttinoni, G. Volpe, F. Kümmel, G. Volpe and C. Bechinger, *J. Phys.: Condens. Matter*, 2012, **24**, 284129.

16 J. Palacci, S. Sacanna, A. P. Steinberg, D. J. Pine and P. M. Chaikin, *Science*, 2013, **339**, 936–940.

17 L. G. Wilson, V. A. Martinez, J. Schwarz-Linek, J. Tailleur, G. Bryant, P. N. Pusey and W. C. K. Poon, *Phys. Rev. Lett.*, 2011, **106**, 018101.

18 V. A. Martinez, R. Besseling, O. A. Croze, J. Tailleur, M. Reufer, J. Schwarz-Linek, L. G. Wilson, M. A. Bees and W. C. K. Poon, *Biophys. J.*, 2012, **103**, 1637–1647.

19 A. Jepson, V. A. Martinez, J. Schwarz-Linek, A. Morozov and W. C. K. Poon, *Phys. Rev. E*, 2013, **88**, 041002.

20 S. Gangwal, O. J. Cayre, M. Z. Bazant and O. D. Velev, *Physical review letters*, 2008, **100**, 058302.

21 K. J. Rao, F. Li, L. Meng, H. Zheng, F. Cai and W. Wang, *Small*, 2015, **11**, 2836–2846.